First in vivo results with 3D Ultrasound Computer Tomography

N.V. Ruiter, M. Zapf, R. Dapp, T. Hopp, H. Gemmeke
Karlsruhe Institute of Technology,
Institute for Data Processing and Electronics,
Karlsruhe, Germany
{nicole.ruiter@kit.edu}

Abstract—**We designed and built a 3D ultrasound computer tomography (USCT) device with a nearly isotropic and spatially invariant 3D point spread function (PSF), to be tested in a clinical study. The objective of this work was to image first healthy volunteers and to evaluate the USCT volumes in comparison to corresponding Magnetic Resonance Images. The here presented volumes are reflectivity images generated with 3D synthetic aperture focusing technique (SAFT). The volunteers were imaged with different parameterization of the data acquisition. The data acquisition time was between four and twelve minutes. For both volunteers we found that the breast structure is clearly delineated in the USCT volume and fit the structures given by the MRI.**

Keywords—ultrasound computert tomography, 3D, in vivo images

I. INTRODUCTION

Breast cancer is the most common type of cancer among women in Europe and North America [1]. Unfortunately, breast cancer is often initially diagnosed after metastases have already developed. A more sensitive imaging method may enable detection in an earlier state to enhance the survival probability of the women.

A promising candidate for sensitive imaging of breast cancer is ultrasound computer tomography (USCT). The possible benefits of USCT have been known for a long time. First publications in this field date back to the 70s, e.g. by Schomberg [2]. The main advantages of a USCT system are simultaneous recording of reflection, attenuation and speed of sound images, high image quality, and fast data acquisition. Due to the defined patient positioning and no breast deformation, the volume images of the female breast are reproducible.

Building such a device for clinical practice was not successful for a long time - mostly due to the huge data rate and the time consuming image reconstruction. Currently, the first 2D and 2.5D systems have become available for clinical evaluation [3,4]. Usually USCT systems implement unfocused ultrasound emission and reception to reconstruct optimally focused reflection images by synthetic aperture post-beamforming. However, most systems are only unfocused in 2D; the elevation dimension is still focused. Such systems lead to large slice thickness with limited depth of field, loss of out-of-plane reflections, and large number of movement steps to acquire a stack of images of the whole volume [4]. 3D USCT, using spherical wave fronts for imaging, overcomes these limitations.

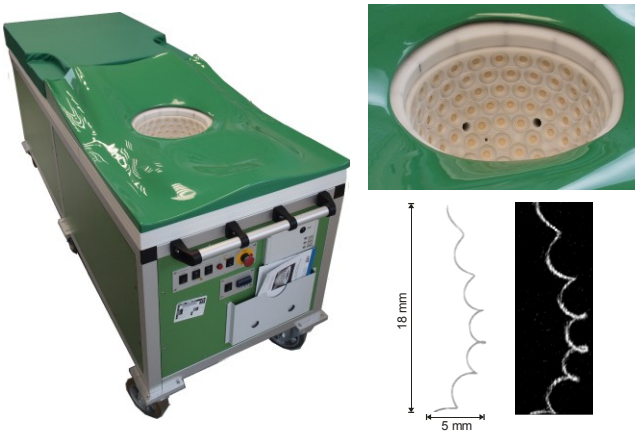

Figure 1. Left: 3D USCT II. Top right: Transducer aperture. Bottom right: 0.07 mm metal thread, photo (left) and maximum intensity projection of a reconstruction (right).

In this paper our current prototype, 3D USCT II, was applied to image the breasts of two healthy volunteers.

II. PROTOTYPE 3D USCT II

An optimized aperture in form of a semi-ellipsoid was developed based on simulations of the isotropy of the 3D point spread function (PSF), the image contrast and the illumination [6]. 3D USCT II has a semi-ellipsoidal aperture with 628 emitters and 1413 receivers. Approx. spherical wave fronts are generated by emitting with a single emitter at 2.4 MHz (50% bandwidth). Rotational and translational movement of the complete sensor system creates further virtual positions of the ultrasound transducers [7]. Data acquired at one of these movements is called “aperture position” in the remainder of this paper. The data acquisition is carried out with an FPGA based system which can store up to 40 GB of A-scans. The digitalization is performed by 480 parallel channels (12 Bit @ 20 MHz), enabling data acquisition of one aperture position in approx. ten seconds.

After digitization, the parallel data streams are processed by the FPGAs of the data acquisition hardware. The data streams are band pass filtered (1.67 to 3.33MHz @ (-60 dB)) and the data rate is reduced by factor 6, performing a band pass undersampling. The reduced data is then stored in the internal 40 GB memory buffer. Using this approach it is possible to store up to 23 aperture positions in one data acquisition process.

The whole device is embedded in a patient bed as shown in Fig. 1. The 3D USCT II has a length of 2 m, a width of 70 cm

and a height of 90 cm. It is covered by a mattress and serves as examination couch. It holds the aperture connected to the data acquisition hardware, translation- and rotation mechanics and motors, power supplies, water reservoir, water heating and disinfection system.

III. Data Preprocessing and Reconstruction

The applied reconstruction algorithm for reflectivity images is the 3D synthetic aperture focusing technique (SAFT), which can be formulated as the following equation:

$$R\ p\ =\ _{j,k}T(A_{j,k}\ t\ p\ \ ) \quad (1)$$

where R denotes the reconstructed qualitative volume of local impedance differences at the reconstruction point p . T describes the preprocessing steps, $A_{j,k}$ is the A-scan acquired at emitting position e_j and receiving position r_k. Norton and Linzer [5] showed that for ideal conditions, i.e. continuous aperture, isotropic point scatterers, no attenuation, SAFT solves the inverse problem of calculating the local impedance differences.

The time t is related to the point p by

$$t\ p\ =\ \frac{p-e_j\ +\ p-r_k}{c(p,e_j,r_k)} \quad (2)$$

For the simplest reconstruction the average speed of sound may be assumed to be constant $c\ p,e_j,r_k\ =c$, e.g. the speed of sound in water at the temperature measured during image acquisition. Alternatively, the mean speed of sound on the path from emitter to point to receiver can be calculated from a speed of sound map of the object.

For the here presented results the speed of sound for each A-scan was calculated from individual temperature measurements at the surface of the transducers, as every transducer system includes a temperature sensor. The temperatures at emitter and receiver were averaged.

The A-scans were preprocessed using a matched filter, followed by envelope, detection of local maxima and convolution with an optimal pulse [8]. The main lobe of the optimal pulse was set to 2 µs to account for the aberrations due to speed of sound variations, which corresponds to a width of the point spread function of approx. 1.5 mm.

The computing system for reconstruction consists of a reconstruction PC (4 x AMD Opteron Octacore, 2.3 GHz, 256 GB RAM) and an external GPU crate (One Stop Systems, OSS-PCIe-2U-ENCL-EXP-4-1) connected via a 16-lane, second generation PCI-Express bus. The external GPU crate is equipped with four Nvidia Geforce GTX 590 cards. With two GF100 GPUs per card (Fermi-Microarchitecture, 1.28 GHz, 1.5 GB RAM), this results in a total number of eight separate CUDA devices for image reconstruction.

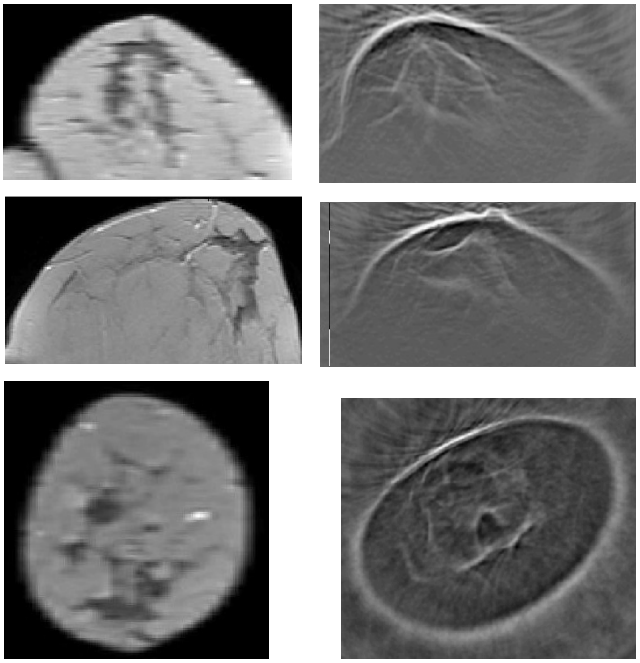

Figure 2. 69-year-old healthy volunteer, D cup. Left: MRI slices in sagittal (top), transversal (left) and frontal (bottom) direction. Right: USCT slices at similar positions .

IV. In Vivo Images of First Volunteers

A. Qualitative comparison to clinical MRI

Fig. 2 shows Magnetic Resonance Images (MRI) and USCT slices of the left breast of a 69-year-old healthy volunteer with a D cup.

The MRI slices were provided by the University Hospital Jena. They are dynamic T1-weighted spoiled gradient echo scans with an in-plane resolution of 0.9 × 0.9 mm, a slice thickness of 3 mm. The time of acquisition was 1 min per measurement, the time of repetition (TR) was 113 ms and the echo time (TE) was 5 ms.

The USCT was acquired at four aperture positions (3.5 million A-scans) in approx. four minutes overall data acquisition time. For emission a linear frequency coded chirp was employed with 2.5 MHz center frequency, 1 MHz bandwidth and 12.8 µs duration. The A-scans were distance amplitude corrected. The SAFT reconstruction was carried out with voxels of $(0.75\ \text{mm})^3$ and took approx. 45 minutes. The volume was gamma corrected before display.

Direct voxel to voxel comparisons between the MRI and the USCT volume without registration were not possible due to differences in patient positioning, e.g. due to the buoyancy of the breast in the water bath of the USCT. For this volunteer the breasts were additionally deformed by the mamma coil of the MRI, which led to a nonlinear deformation with a non-central nipple position in the MRI, see e.g. transversal MRI slice in Fig. 2.

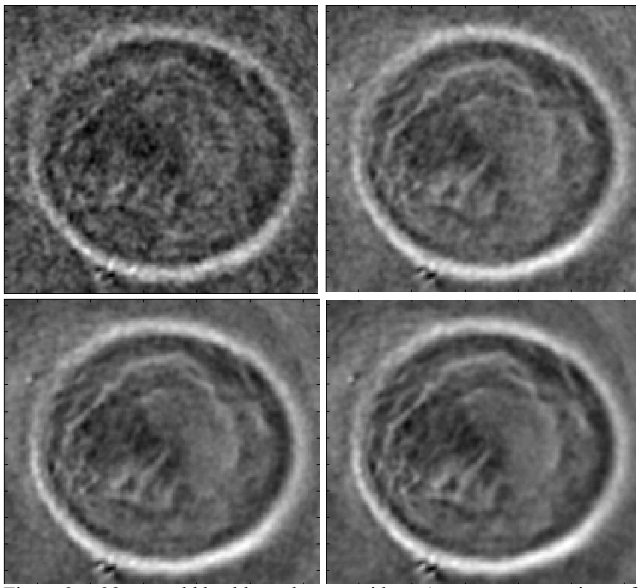

Figure 3. 38-year-old healthy volunteer with an A cup: reconstructions of a frontal slice for one, four, eight and sixteen aperture positions from top left to bottom right. The slices are 11 cm by 12 cm and 3 cm inside the breast measured from the nipple position.

In general, we found that the outline and structure of the breast is clearly delineated in the USCT volume. The overall shape and internal tissue structures fit the structures given by the MRI. The glandular tissue (grey in the MRI slices and bright in the USCT slices) have approximately the same shape and show the typical tree like structure toward the nipple The PSF is isotropic in all directions. The contrast of the structures towards the chest wall is slightly decreasing. The contrast of the inner structures seems acceptable, however, grating lobes are clearly visible, especially outside the breast, and might lead to superposition of small weak scattering internal structures

B. Parameter study: Object contrast vs. apertur positions

For this parameter study the right breast of a 38-year-old healthy volunteer with an A cup was imaged. To decrease the sparseness of the aperture, i.e. to decrease the grating lobes and increase the contrast, the data was acquired at 16 aperture positions (14 million A-scans) in 12 minutes. Again the linear frequency coded chirp was employed (see subsection *A.*). The SAFT reconstruction was carried out with voxels of $(0.75\ \text{mm})^3$. For each aperture position one USCT volume was reconstructed. The overall reconstruction time was approx. 3 hours.

Fig. 3 shows the reconstruction of a frontal slice for one, four, eight and sixteen aperture positions. The contrast of the inner structures against the noise increases and the details get more visible with increasing aperture positions. The noise outside the breast loses the grained structure and becomes much smoother.

In order to evaluate the contrast gain quantitatively, the contrast was evaluated in terms of peak-signal-to-noise-ratio:

$$PSNR = 20\log_{10}\frac{\max(X)}{\sigma(X')}, \qquad (3)$$

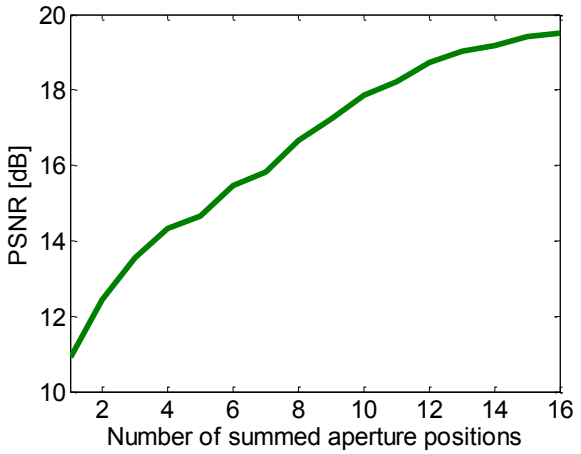

Figure 4. PSNR values over increasing number of aperture positions.

where X is region of interest inside the reconstructed breast, X' a region of interest outside the breast, *max* the maximum operator and σ the standard deviation. The breast was reconstructed for each of the 16 aperture positions and the PSNR was calculated for successive sums of these volumes. To normalize the comparison the maximum was evaluated at the same image point, which was defined by the maximum of X for the sum of all 16 positions. Fig. 4 shows the PSNR values over increasing number of aperture positions.

The PSNR was calculated for X as a cuboid volume of 5.5 cm x 6 cm x 3.5 cm inside the reconstructed breast excluding the skin. The PSNR represents the maximum contrast inside the breast tissue without the predominant skin.

X' was a region of interest of 6.5 cm x 5 cm x 4.5 cm outside the breast to approximate the background noise. Grating lobes increase with distance from the center of the volume [9]. Therefore, X' overestimates the background noise generated by the grating lobes inside the breast slightly.

The PSNR increases steadily with the number of summed aperture positions by approx. 10 dB, fitting the subjective impression when viewing the slice images. The PSNR curve appears to slowly saturate starting at approx. 10 summed aperture positions, but more positions than 16 might increase the image contrast further. Also, as the PSNR uses only the maximum value of a signal, more details might become visible.

C. Detail reconstruction

The resolution of the current images is limited by the aberrations due to the speed of sound variations. To get an impression of a higher resolution image, the reconstruction was done for the tip of the breast which moderates the aberration effects. Fig. 5 shows a reconstruction of the dataset presented in subsection *B* with the main lobe of the optimal pulse set to 1 µs, which corresponds to a width of the point spread function of approx. 0.75 mm. The SAFT reconstruction was carried out with voxels of $(0.38\ \text{mm})^3$ using 16 aperture positions. The reconstruction time was around 5 h.

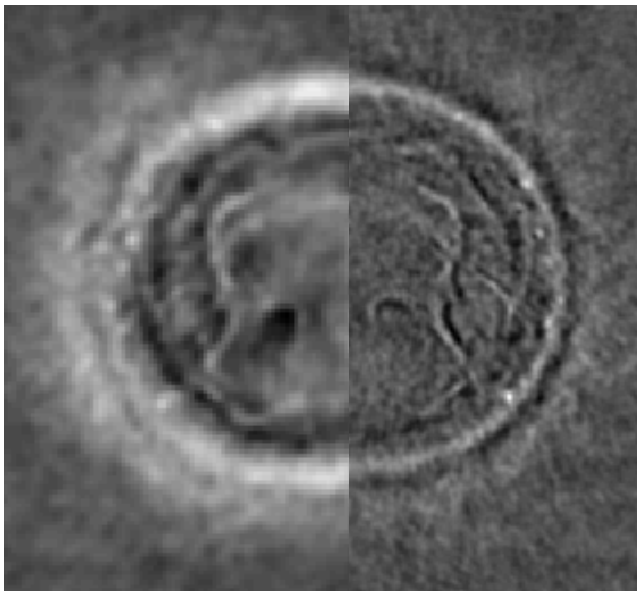

Figure 5. Frontal slices 1.8 cm inside the breast measured from the nipple position. Left: Lower resolution reconstruction. Right: Higher resolution reconstruction (mirrored).

As expected the skin und inner tissue structure in the detail reconstruction is displayed with higher resolution. The tissue surfaces are appearing sharper and more details are visible.

V. DISCUSSION AND CONCLUSION

In this paper first volunteer reconstructions of in vivo data with our 3D USCT II device have been presented. For both volunteers we found that the breast is clearly delineated in the USCT volume. The overall shape and internal tissue structures of the first volunteer fit the structures given by the MRI. Data acquisition and reconstruction of more aperture positions, i.e. with a less sparse aperture, increase the contrast of the breast's inner structures. The level of detail displayed for the inner structures of the second volunteer for 16 aperture positions seems realistic. As the second volunteer has only an A-cup the lateral parts of the breast were not inside the aperture. Due to the spherical emission and reception, a part of the volume reconstruction could be done outside the aperture. Here also the pectoral muscle gets visible, which is valuable diagnostic information and another advantage compared to 2D systems.

Due to the phase aberrations caused by speed of sound variations the reconstructions are limited in resolution, i.e. 1.4 mm. In a next step the speed of sound variations will be included in the SAFT reconstruction as indicated in eq. (2), which will allow to use the full resolution of up to $(0.2\ \text{mm})^3$ for reflectivity imaging .

Patient movement seems to be a minor problem; no definite movements between reconstructions of the single aperture positions could be detected (data acquisition time at one position is approx. ten seconds). Breathing movement of the volunteers seems to be not transported to the breast. The duration of the data acquisition of up to 12 minutes was reported to be (easily) bearable for the volunteers.

The next step in this work is to carry out a clinical study with patients.

REFERENCES

[1] T. Fischer, U. Bick, A. Thomas, "Mammographie-Screening in Deutschland," Visions Journal (15), 2007.

[2] H. Schomberg, "An improved approach to reconstructive ultrasound tomography," J. Phys. D: Appl. Phys. 11, 1978.

[3] N. Duric, P. Littrup, et al., "Detection of breast cancer with ultrasound tomography: First results with the computerized ultrasound rrisk evaluation (c.u.r.e.)," Medical Physics 34(2), 2007.

[4] J. Wiskin, D. Borup, et al., "Inverse scattering and refraction corrected reflection for breast cancer imaging," Proc. SPIE Medical Imaging, 2010.

[5] S. Norton, M. Linzer, "Ultrasonic reflectivity imaging in three dimensions: Reconstruction with a spherical array," Ultrasonic Imaging 1, 1979.

[6] G. Schwarzenberg, M. Zapf, et al., "Aperture optimization for 3D ultrasound computer tomography," in Proc. IEEE Internat. Ultrasonics Symp, 2007.

[7] H. Gemmeke, A. Menshikov, et al., "Hardware Setup for the Next Generation of 3D Ultrasound Computer Tomography," Proc. IEEE NSS MIC 2010.

[8] N.V. Ruiter, G.F. Schwarzenberg, et al., "Improvement of 3D ultrasound computer tomography images by signal pre-processing," Proc. IEEE Internat. Ultrasonics Symp., 2008.

[9] F. Simonetti, L. Huang, N. Duric, "On the sampling of wave fields with circular ring apertures," Journal of applied physics, 101, 2007.